


Research Article

A Comparative Study between Polyline and Straight Line Arrangements of Antislid e Piles Based on Soil Arching Effect

Xue-gang Dai,¹ A. Fa-you ,^{1,2} Peng Zhang,¹ and Shi-qun Yan¹

¹Faculty of Land Resource Engineering, Kunming University of Science and Technology, Kunming, Yunnan 650093, China

²Key Laboratory of Geohazard Forecast and Geocological Restoration, Plateau Mountainous Area, Ministry of Natural Resources of the People's Republic of China, Kunming, Yunnan 650000, China

Correspondence should be addressed to A. Fa-you; afayou@163.com

Received 5 July 2022; Accepted 27 September 2022; Published 14 October 2022

Academic Editor: Zhixiong Zeng

Copyright © 2022 Xue-gang Dai et al. This is an open access article distributed under the Creative Commons Attribution License, which permits unrestricted use, distribution, and reproduction in any medium, provided the original work is properly cited.

Considering the limitations of terrain and engineering expenses, antislid e piles are sometimes arranged in polylines. Studies show that this arrangement adversely affects the mechanical characteristics of antislid e piles. However, there is no in-deep understanding of this issue and the structural design and calculation method of this arrangement have not been discussed in relevant standards. Aiming at resolving this shortcoming, the polylines pile arrangement is studied in this article to provide a scientific basis for designing and calculating antislid e piles. To this end, the cantilever pile is taken as the research background, and the soil arching effect between piles is taken as the research object. Then the performances of the single-row polyline pile layout and straight line pile layout are analyzed in the Dawanjiang landslide and the results are verified from the aspects of the landslide reinforcement and the influence on the antislid e pile structure. The obtained results show that the polyline pile layout is disadvantageous to the safety of the antislid e pile structure, and the soil arch between piles under the polyline pile layout condition is not uniform. Meanwhile, it is found that as the polyline pile layout angle increases, the stress concentration appears at the “inflection point.” Under this circumstance, the soil arch between piles is not uniform, and the stress concentration intensifies.

1. Introduction

Pile is a civil engineering structure with a long history, which has been used for more than 14,000 years. With the development of science and technology, piles have been made of cast-iron sheets, steel, cement, concrete, and reinforced concrete [1–3]. With the rapid development of engineering construction, pile foundation has been widely used in housing construction, bridge wharf, and managing geological disasters. Recently, numerous investigations have been carried out on the design theory, construction technology, testing technology, and application of piles in diverse applications [4–6].

Landslide is one of the most catastrophic natural geological disasters in the world. The study of landslide formation and prevention methods has attracted many scholars worldwide [7, 8]. In this regard, antislid e piles have notable

antislid e characteristics, low sewage works, flexible arrangement, convenient construction, and good treatment effect. Accordingly, investigating the antislid e pile has become a research hotspot. A review of the literature indicates that numerous investigations have been carried out on antislid e piles from different aspects. However, most investigations have been focused on the bearing mechanism of antislid e piles [9–11] and developing modified design and calculation methods [12, 13]. Studies show that the plane layout of an antislid e pile, including the position of the pile and the distance between the piles, significantly affects the pile performance and stability of the structure. Li et al. [14] developed an interval model for stabilizing piles based on the friction soil arching effect. Moreover, Li et al. [15] proposed a simplified analytical model to analyze double-row pile stabilized slopes. Liu et al. [16] improved the plane layout of stabilizing piles based on the piecewise function expression

of the irregular driving force. Zhang et al. [17, 18] proposed a method to calculate the maximum and minimum pile spacing considering the soil arching effect and interactions between multilayered sliding masses. Li et al. [19] developed a mechanical model of the soil arch to investigate interactions between piles and slope and optimize the pile spacing. Regarding the plane layout of antislides piles, a straight line arrangement is mainly adopted to ensure the antisliding effect, where the piles are arranged perpendicular to the landslide thrust direction. However, due to the limitations of terrain conditions and engineering investment in actual engineering, the antislides piles are sometimes arranged in polylines as well. The biggest feature of polyline layout is that the antislides piles are distributed in polylines on the plane. That is, some antislides piles are arranged perpendicular to the landslide thrust direction, while the other part of the piles is arranged obliquely to the landslide thrust direction (Figure 1). Currently, although polyline layout is commonly used in landslide control, its kinetic mechanism is unclear, and the design and computational methods for pile structures have not been explained in relevant regulations. Hence, mechanism research is required to investigate the overall antisliding and soil arching effects of polyline layout, as well as its influence on the internal force distribution of antislides pile bodies.

As a major index reflecting the antisliding effect of piles, the soil arching effect refers to the stress redistribution caused by the heterogeneous displacement of soil under the pile-soil interaction. By transferring the landslide thrust to the antislides piles via the cohesion between soil bodies, it can fully exploit the soil shear strength to enhance the antisliding effect [20]. The discovery of the “granary effect” in 1884 by Roberts [21] marks the earliest research on the soil arching effect. Since 1943, when Terzaghi, a famous geomechanical scientist, confirmed the presence of the soil arching effect through the “Trapdoor test” [22], scholars around the world have paid attention to the research concerning the soil arching effect, achieving fruitful outcomes. Wang et al. [23] studied the soil arching in slopes. Furthermore, Zhang et al. [24–26] studied landslides in the reinforced soil arch by antisliding piles. Bosscheret al. [27, 28] studied the soil arch in Sandy. Deb et al. [29, 30] established a soil arch model. Moreover, numerous indoor model tests [31–33] and numerical simulations [34–36] have been carried out to investigate soil arching. However, none of the extant studies has involved the soil arching effect under polyline pile arrangement, which is worthy of further research. Analyzing the above statements, it can be noted that the design of polyline pile arrangement is a very topical issue. Therefore, the purpose of this study is to provide a corresponding scientific basis for the design of the polyline arrangements of antislides piles, and to achieve this, it is necessary to solve the following tasks:

- (1) Studying the soil arching effect under polyline pile arrangement. And studying the evolution characteristics differences of soil arching effect in straight lines from those arranged in polylines.
- (2) Revealing the risks of the polyline arrangements of antislides piles.

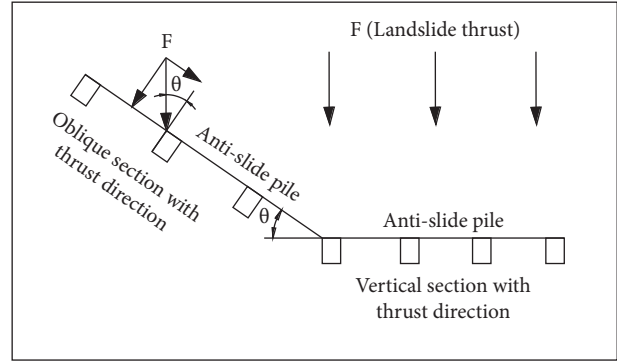


FIGURE 1: Schematic of polyline pile arrangement (made by the authors).

2. Soil Arch Calculation Model

2.1. Basic Hypotheses. Soil arching effect is a 3D space problem with complex stress relationships, which is caused by the heterogeneous displacement between soil particles under the action of landslide thrust. During analysis in this study, the soil arching effect is transformed into a plane strain problem and the following hypotheses are made:

- (1) The thrust of landslide behind piles is a uniform load, where the resistance of soil in front of piles and the lateral pressure of soil are disregarded;
- (2) The influences of arch thickness and soil self-weight are disregarded, and the soil arch is a single line type;
- (3) The soil arching problem is assumed as a plane strain problem, and the arch shape variation with depth is disregarded.

2.2. Equation for Reasonable Arch Axis. Reasonable axis of soil arch means that when the soil arching effect is optimal, the structure and shape of soil arch are inevitably in the most reasonable stress state, which is called the reasonable arch axis in structural mechanics. There is no bending moment or shear force on any section on the reasonable arch axis, where only the axial force exists.

As is clear from the force diagram of soil arch in Figure 2, the force F on the arch back is a uniform load, b denotes the width of each antislides pile, L denotes the net distance between piles, p_x, p_y, p_h and p_v represent the end reactions of piles to the soil arch in the X and Y directions, and f is the soil arch vector height. Since the bending moment at any point on the reasonable arch axis equation is 0, the balance equation is established for the moment at arbitrary point N as follows:

$$\frac{F}{2}x^2 - P_x y + P_y x = 0. \quad (1)$$

According to the force balance in the X direction:

$$P_v = P_x. \quad (2)$$

According to the force balance in the Y direction:

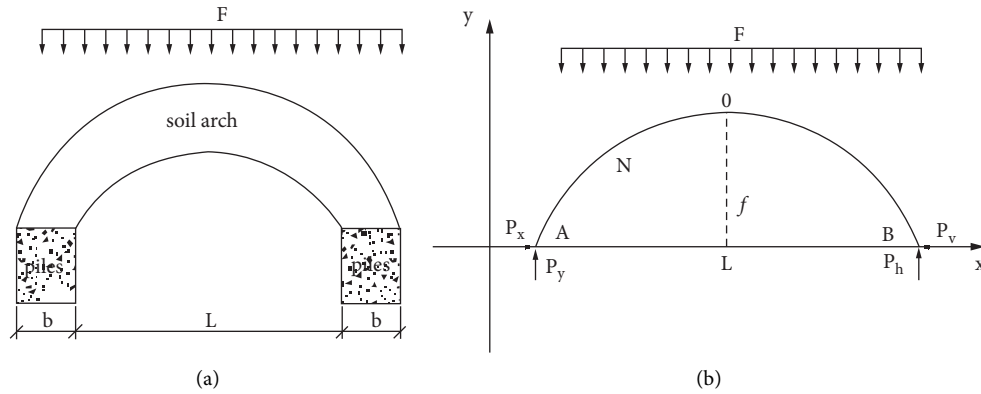


FIGURE 2: Force diagram of soil arch [37].

$$p_y = \frac{L}{2}F. \quad (3)$$

By taking the moment at point O , the balance equations are established as follows:

$$\frac{F}{8}L^2 - \frac{F}{4}L^2 + P_x f = 0 \quad (4)$$

$$P_x = \frac{F}{8}L^2.$$

Accordingly, the equation for soil arch axis is given as follows:

$$y = \frac{4fx(L-x)}{L^2}. \quad (5)$$

At any point M on the axis of symmetrical soil arches, the vertical support force is F_x , the horizontal thrust is $p_x = F/8L^2$, and the resultant force O is given as follows:

$$O = \frac{F\sqrt{L^2 + 64x^2 f^2}}{8f}. \quad (6)$$

The azimuth angle α of soil arch line is expressed as follows:

$$\alpha = \tan^{-1} \left[\frac{8fFx}{FL^2} \right] = \tan^{-1} \left[\frac{8fx}{L^2} \right] = \tan^{-1} \left[\frac{dy}{dx} \right]. \quad (7)$$

It is clear from Equation (7) that the resultant force O at any point is precisely the axial force. According to Equation (7), the resultant force O at any point is the increasing function of x . That is, the minimum axial force at the arch crown is $L^2/8ff$, and the maximum axial force at the arch foot is $FL\sqrt{L^2 + 16f^2}/8f$. Hence, on the premise of the abovementioned hypotheses, failure of soil arch occurs initially at the foot position.

3. Comparative Analysis of Soil Arching Effect Simulations

Formation of soil arching effect is attributed to the principal stress migration, in which the soil body transfers the landslide thrust to the nearby area of pile periphery soil by

relying on the shear strength between soil particles under the pile-soil interaction. Thus, the strength of soil arching effect can be determined by the deflection degree of stress between soil particles. Stronger soil arching effect indicates greater deflection of principal stress and a more obvious decrease of landslide thrust along the negative direction of the Y -axis (landslide thrust direction). Unlike the ordinary arch structure, the soil arch is a stress arch generated inside the soil body. Its action and nonaction zones have the same medium, making it difficult to determine a clear boundary. Meanwhile, given the coincidence of the intersection point between the reasonable axis and midspan symmetry plane of soil arch with the stress peak point in the X direction, the straight line distance from this point to the rear of antislid piles along the Y direction is precisely the vector height of soil arch. Thus, the change in soil arching effect range can be analyzed based on the variation of arch vector height. Besides, the extrusion strength between soil particles is determined according to the size of X -directional principal stress on the midspan symmetry plane of soil arch. Greater value of X indicates stronger soil extrusion effect and higher arch strength. In summary, during the analysis of soil arching effect in this study, the principal stress distribution isogram in the Y direction, and the X - and Y -directional principal stress distribution curves on the midspan symmetry plane of soil arch are mainly analyzed, in order to compare the evolution of soil arching effect under straight line layout versus that under polyline layout.

In this section, fast lagrangian analysis of continua in 3 dimensions (FLAC3D) software, which is a powerful tool to perform geotechnical analyses of soil, rock, groundwater, constructs, and ground support [38, 39] is applied to carry out numerical analyses. Studies show that FLAC3D software has remarkable advantages. First, it uses the "mixed discrete method" to simulate plastic failure and plastic flow. It is worth noting that this method is more accurate than the "discrete integration method," which is usually used in the finite element method. Second, even though the simulated system is static, the dynamic equations of motion should be solved, which makes FLAC3D have no numerical obstacles in simulating the physically unstable process. Last, it adopts an explicit solution scheme. Therefore, the explicit solution takes almost the same time to obtain the nonlinear stress-

strain relation as the linear constitutive relation, while the implicit solution takes a long time to solve a nonlinear problem. Meanwhile, there is no need to store the stiffness matrix so multielement structures can be solved with less memory capacity. Therefore, it is feasible to simulate large deformations because there is no stiffness matrix to be modified. Accordingly, the FLAC3D software is selected in the present study to analyze the problem.

During numerical analysis, a geological model of an ideal landslide is built based on FLAC3D while ignoring the changes in surface configuration. Figure 3 displays the typical section of the homogeneous soil landslide. To eliminate the influence of boundary conditions, the model boundary before the piles is extended to 20 m, while that behind the piles is extended to 30 m during modeling. The self-weight load is primarily considered in the calculation herein, and unidirectional constrained boundaries are adopted on the two sides and bottom of the model. Regarding the soil constitutive model, the Mohr–Coulomb plasticity model following Mohr–Coulomb yield criterion is adopted, while the elastoplastic model is employed for the antislides piles and retaining plates. Table 1 details the computational parameters.

3.1. Numerical Simulation of Straight Line Pile Arrangement

3.1.1. Modeling. Figure 4 depicts the ideal model for a straight line layout of piles, which is 64.4 m long, 40 m wide, and 14 m high. The slide body has a thickness of 6 m. The model is divided into 277,344 meshes, and a total of 9 antislides piles are set up, with a length of 10 m, where the anchoring section is 6 m below the pile top. The pile cross section is 2 m long, 1.5 m wide, and the pile spacing is 6 m. Retaining plates are provided behind the antislides piles, which are 6 m long, 6 m wide and 0.5 m thick. For the model, its right side is the positive direction of the X -axis, its rear side is the positive direction of the Y -axis, and its top side is the positive direction of the Z -axis.

During the investigation of soil arching effect, the action zone of the 5 antislides piles in the middle is selected for the study. The corresponding soil arches are the 3# soil arch between 3#–4# piles, the 4# soil arch between 4#–5# piles, the 5# soil arch between 5#–6# piles, and the 6# soil arch between 6#–7# piles. Disregarding the changes in soil arches in the vertical direction, the horizontal section at $Z = 8$ m is taken for analysis.

3.1.2. Analysis of Simulation Results. Figures 5 and 6 separately display the displacement and principal stress isoline maps in the Y direction under a straight line layout of piles. By analyzing the displacement and stress distribution of soil behind the piles, we can determine whether the soil arching effect occurs, and can reflect the deflection of landslide thrust and the action range of soil arches. It is clear from Figure 5 that the displacement of soil between the piles is significantly larger than that of soil behind the piles. That is, heterogeneous displacement is present between the particles of the slide body. In Figure 6, the Y -directional principal

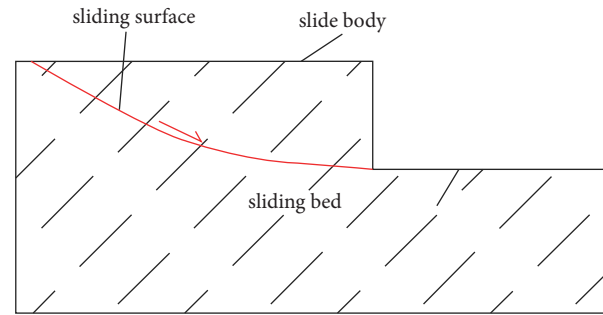


FIGURE 3: Schematic of a typical cross-section of ideal landslide (made by the authors).

stress at the arch midspan decreases gradually from the back to the front of the piles, while the stress value on the back side of the piles increases gradually. This indicates that the Y -directional principal stress along the landslide thrust direction is deflected to both sides and concentrated near the back of the piles. Based on the formation conditions and mechanism of soil arches, it can be determined that the soil arching effect already occurs under the straight line layout. Besides, according to the principal displacement and stress distribution in the figure, under the straight line layout, the action ranges of 3#, 4#, 5#, and 6# soil arches are basically identical. The closer the principal stress to the sheet-pile wall vicinity, the more obvious the stress deflection, which is manifested as the greater isoline density on the stress isoline map. Contrastively, as the distance from the wall increases, the isoline density gradually decreases, the thickness of the isobaric zone increases, and the abrupt stress change becomes unobvious. This indicates that the farther away from the sheet-pile wall, the weaker the soil arching effect.

Figures 7, and 8 separately depict the Y - and X -directional principal stress distributions on the midspan symmetry plane of soil arches under the straight line pile arrangement. As is clear, the forces and action ranges are basically identical for the 3#, 4#, 5#, and 6# soil arches. In Figure 7 the Y -directional principal stress decreases most obviously in the $X = 0.5$ – 4.9 m region, and in Figure 8, the X -directional principal stress also reaches its peak in this region, suggesting that this region is the range of soil arching effect. Besides, it is clear from Figure 7 that at $X = 1.95$ m, the principal stress value peaks, that is, the vector heights of soil arches are all 1.95 m.

In summary, the soil arching effect can be produced when the piles are arranged in straight lines, which weakens gradually along the direction against the antislides piles. Meanwhile, the forces and action ranges are basically identical for the 1#, 2#, 3#, and 4# soil arches. This suggests that under a straight line layout, the landslide thrust is uniformly distributed at various positions, and the antislides sheet-pile walls evenly share the load, which is beneficial to the safety of sheet-pile wall structure.

3.2. Numerical Simulation of Polyline Pile Arrangement

3.2.1. Modeling. To investigate the evolution characteristics of soil arching effect under the polyline arrangement of piles, a model of polyline pile layout is built (Figure 9), with which

TABLE 1: Physicomechanical parameters of materials.

| Model material | Elastic modulus E (GPa) | Poisson's ratio μ | Internal friction angle φ (°) | Cohesion C (kPa) |
|-----------------|-------------------------|-----------------------|---------------------------------------|------------------|
| Soil body | 0.02 | 0.25 | 15 | 17 |
| Antislid pile | 30 | 0.2 | — | — |
| Retaining plate | 0.3 | 0.2 | — | — |

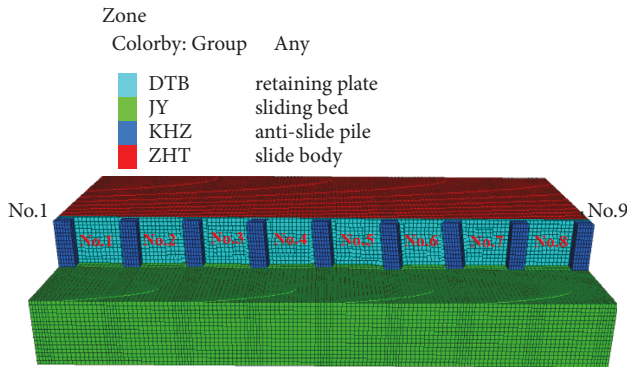


FIGURE 4: Model of straight line pile arrangement.

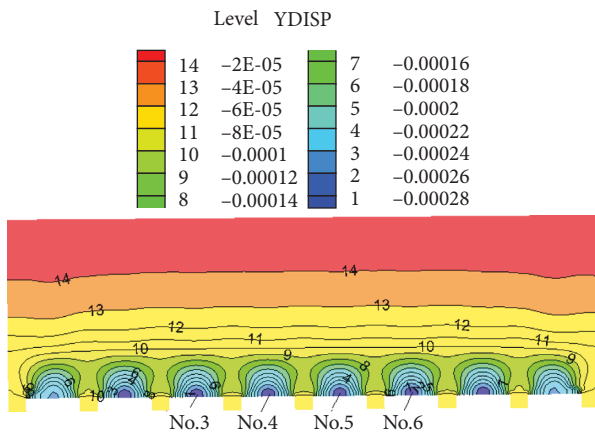


FIGURE 5: Displacement isoline map in the Y direction.

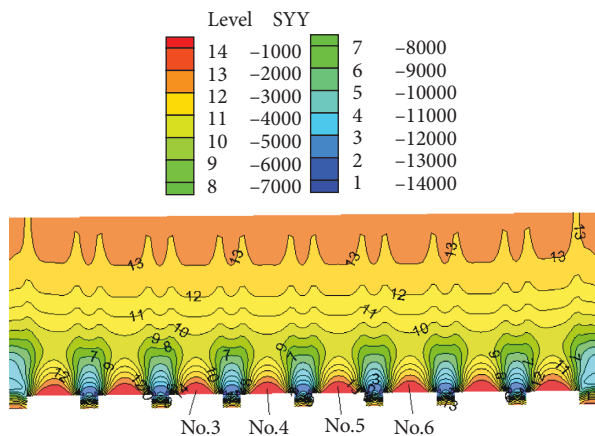


FIGURE 6: Principal stress isoline map in the Y direction.

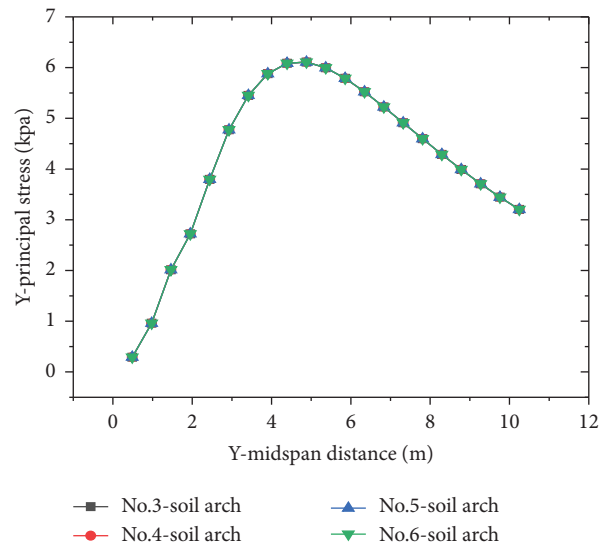


FIGURE 7: Y-directional principal stress curve at midspan of soil arch.

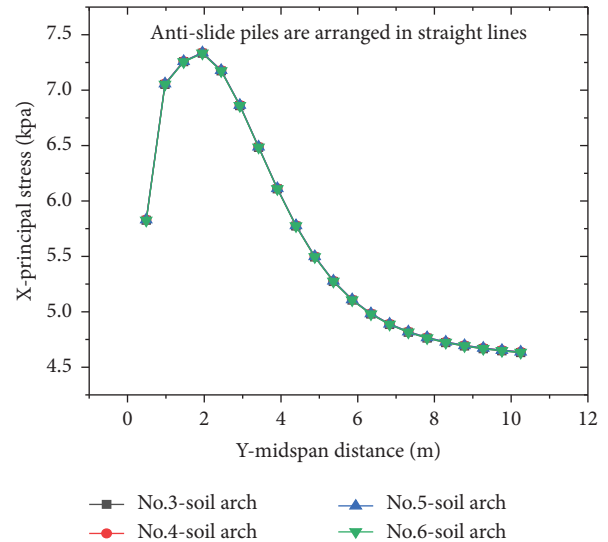


FIGURE 8: X-directional principal stress curve at midspan of soil arch.

the numerical simulation analysis is performed on the soil arching effect between piles. Compared to the afore-described straight line layout, the parameters of the polyline pile layout model remain unchanged except for the adjusted layout angle of the antislid piles. On the basis of a straight line layout, a “section orthogonal to thrust” is arranged for the antislid piles on the right of 5# pile, which serves as the

FLAC3D 5.00
©2012 Itasca Consulting Group, Inc.

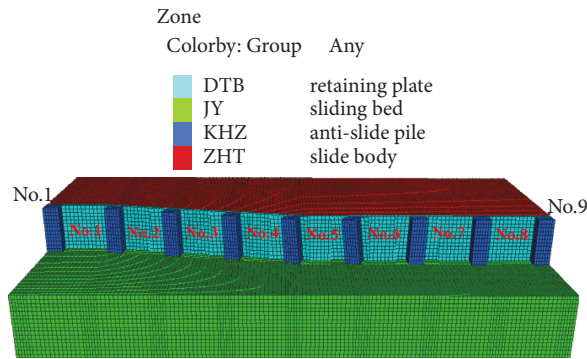


FIGURE 9: Model of 10° polyline pile arrangement.

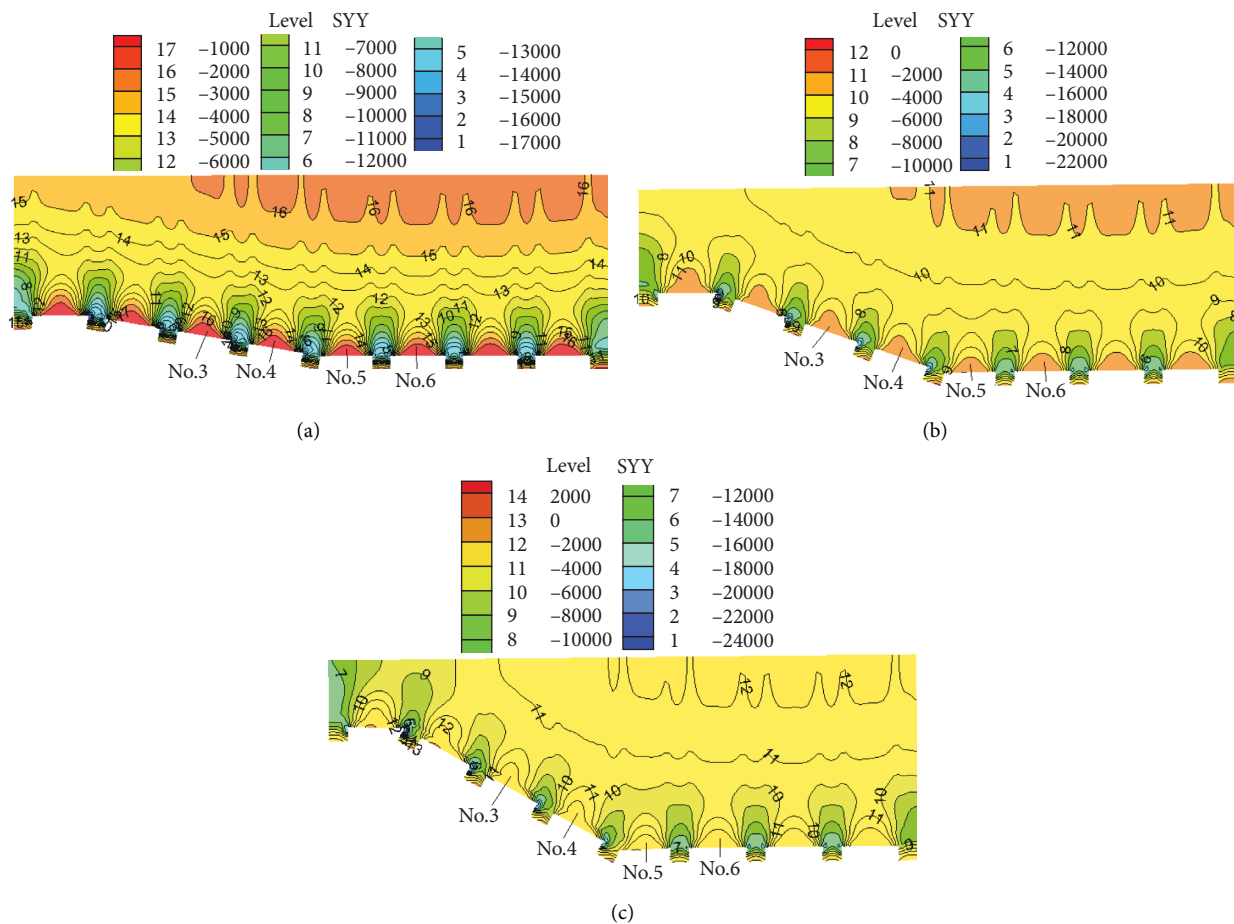


FIGURE 10: Comparisons among principal stress isoline maps in the Y direction, (a) 10° polyline pile arrangement, (b) 20° polyline pile arrangement, and (c) 30° polyline pile arrangement.

inflection point. This section is consistent with that under the straight line layout. Meanwhile, the part on the left of 5# pile is a “section oblique to thrust,” which is overall arranged by rotating at a certain angle with the central point of 5# pile as the circle center. The antislides piles in this section are obliquely intersected with the landslide thrust. In this study, models of 10°, 20°, and 30° polyline pile layouts are separately built. Figure 9 displays the model of 10° polyline pile arrangement.

3.2.2. *Analysis of Simulation Results.* For the convenience of analysis, during the investigation of the soil arching effect under polyline pile arrangement, the soil arches are classified into those on the “section oblique to thrust” and those on the “section orthogonal to thrust.” The 3# and 4# soil arches are on the “section oblique to thrust,” whereas the 5# and 6# soil arches are on the “section orthogonal to thrust.” Besides, the 5# arch is also called the “inflection point” soil arch, since it is very close to the inflection point.

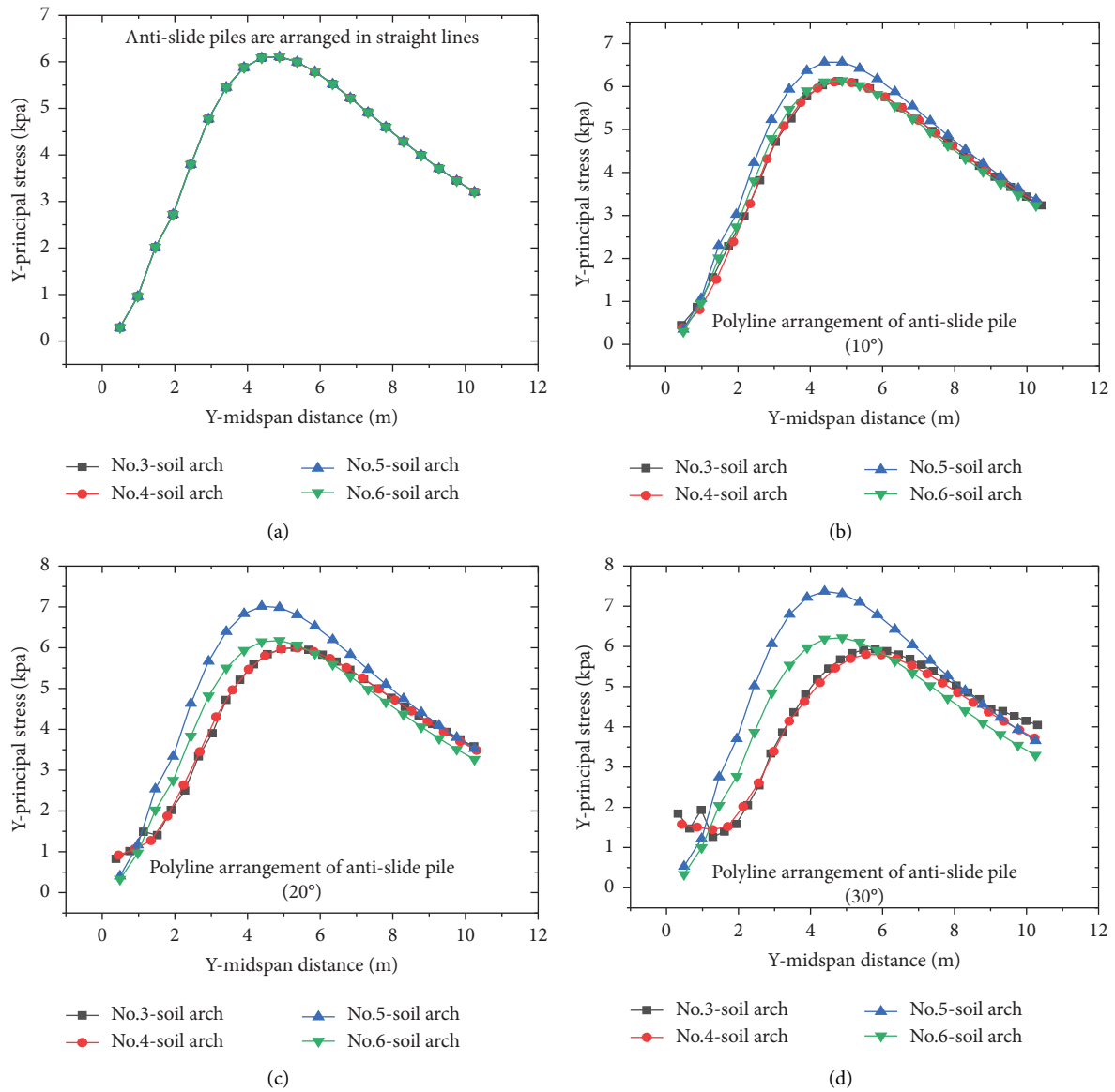


FIGURE 11: Comparisons among principal stress curves in the Y direction.

Figure 10 illustrates the isoline maps of Y-directional principal stresses under the 10°, 20°, and 30° polyline pile arrangements, while Figure 11 presents the comparisons among Y-directional principal stress curves at the midspan under the straight line and 10°, 20°, and 30° polyline pile arrangements. As is clear, the Y-directional principal stress values of soil arches at the midspan gradually decrease from the back to the front of piles, while the stress values on the back side of piles gradually increase. There are clear trajectories of principal stress deflection, indicating that the soil arching effect is exerted. However, unlike the case of straight line layout, under the polyline pile arrangement at the same angles, the Y-directional principal stresses of both 3# and 4# soil arches decrease, while those of both 5# and 6# soil arches increase, especially for the 5# arch. That is, when the piles are arranged in polylines, the soil pressures at the arch crown

within the “section oblique to thrust” decrease, while those within the “section orthogonal to thrust” increase. Such an increase is most evident for the soil arch at the inflection point. Moreover, with the increasing angle of polyline pile layout, the Y-directional principal stress at the “inflection point” increases more evidently. Meanwhile, the principal stresses in the Y direction also differ by the angle of polyline pile layout. Specifically, with the increase in such angle, the isoline density of Y-directional principal stress gradually decreases, the thickness of the isobaric zone gradually thickens, and the progressive decrease of stress is unobvious, suggesting the gradual weakening of soil arching effect.

Table 2 lists the peak statistics for the Y-directional principal stresses of soil arches at various pile layout angles, whereas Figure 12 depicts the variations of Y-directional principal stresses of soil arches at various pile layout angles.

TABLE 2: Peak statistics for the Y-directional principal stresses of soil arches.

| Pile layout angle | Y-directional principal stress peak (kPa) | | | | Peak position | | | |
|----------------------|---|--------------|--------------|--------------|---------------|--------------|--------------|--------------|
| | 3# soil arch | 4# soil arch | 5# soil arch | 6# soil arch | 3# soil arch | 4# soil arch | 5# soil arch | 6# soil arch |
| Straight line layout | 6.11 | 6.11 | 6.11 | 6.11 | 4.9 | 4.9 | 4.9 | 4.9 |
| 10° layout | 6.1 | 6.09 | 6.57 | 6.14 | 4.8 | 5.1 | 4.4 | 4.9 |
| 20° layout | 6 | 5.96 | 7.01 | 6.17 | 5.2 | 5.3 | 4.3 | 4.9 |
| 30° layout | 5.92 | 5.8 | 7.37 | 6.22 | 5.8 | 5.5 | 4.3 | 4.9 |

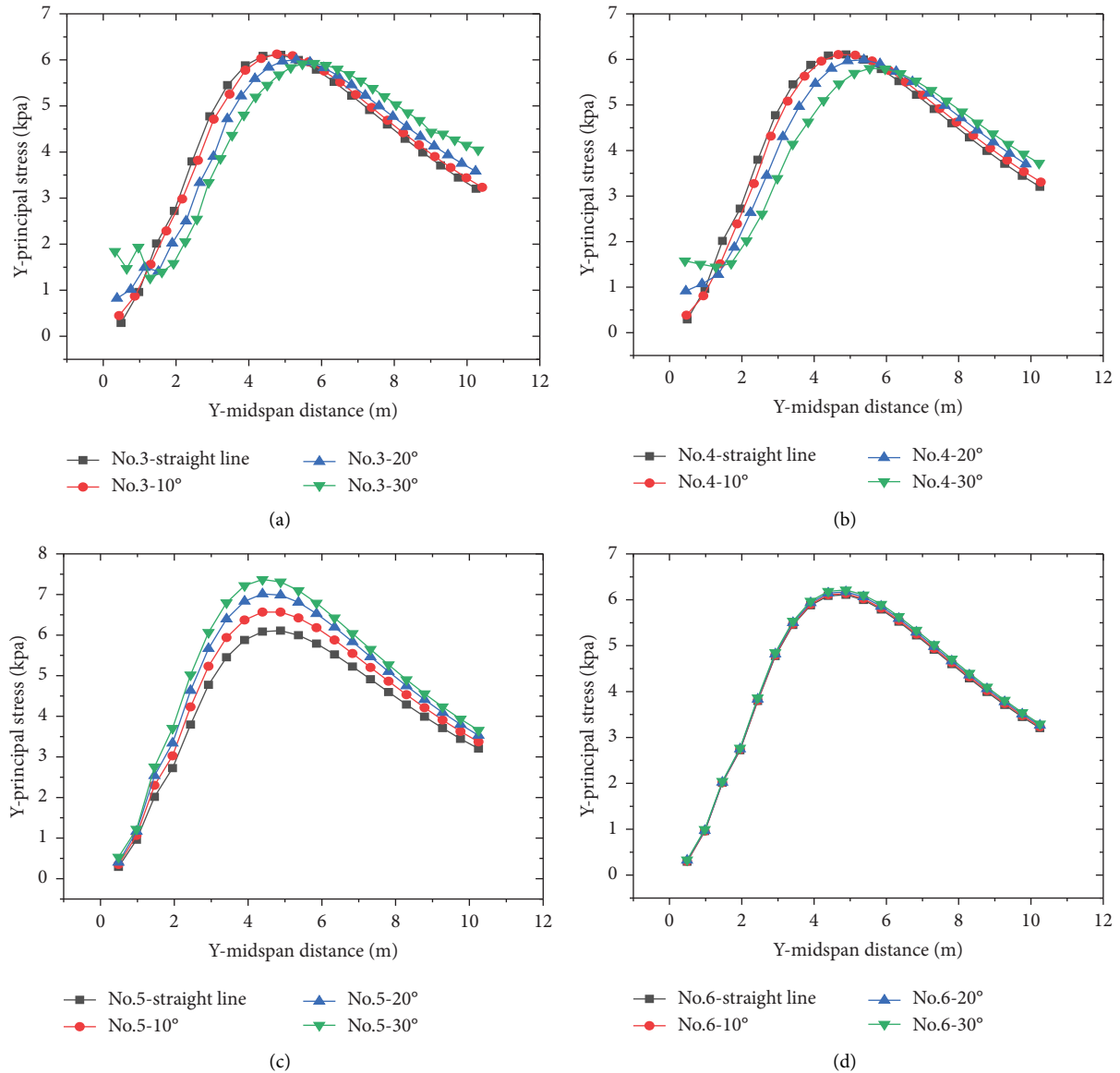


FIGURE 12: Variation curves of Y-directional principal stresses of soil arches at various pile layout angles.

As is clear, with the increase in the angle of polyline pile arrangement, the Y-directional principal stresses on the midspan symmetry planes of 3# and 4# soil arches decrease continuously, while those of 5# and 6# soil arches increase continuously. In addition, with the increase in the angle of polyline pile arrangement, the Y-directional principal stress peaks at the midspan of 3# and 4# arches move backward to varying degrees, suggesting that the range of soil arching

effect shifts away from the antislide piles. Meanwhile, as displayed by the variation curves of Y-directional principal stresses, the inscribed slopes of the curves are gradually decreasing, indicating the weakening of the soil arching effect. The Y-directional principal stress peaks at the midspan of 5# soil arch move forward to varying degrees with the increase in the pile layout angle, suggesting the diminishing range of soil arching effect. Regarding the changes

TABLE 3: Peak and vector height statistics for the X-directional principal stresses of soil arches.

| Pile layout angle | X-directional principal stress peak (kPa) | | | | Vector height (m) | | | |
|----------------------|---|--------------|--------------|--------------|-------------------|--------------|--------------|--------------|
| | 3# soil arch | 4# soil arch | 5# soil arch | 6# soil arch | 3# soil arch | 4# soil arch | 5# soil arch | 6# soil arch |
| Straight line layout | 5.5 | 5.5 | 5.5 | 5.5 | 1.95 | 1.95 | 1.95 | 1.95 |
| 10° layout | 6.92 | 7.29 | 7.73 | 6.14 | 2.17 | 2.33 | 1.46 | 1.95 |
| 20° layout | 7.3 | 7.7 | 8.4 | 7.26 | 2.27 | 2.24 | 1.46 | 1.95 |
| 30° layout | 8.4 | 8.8 | 9.41 | 7.27 | 2.25 | 2.56 | 0.97 | 1.95 |

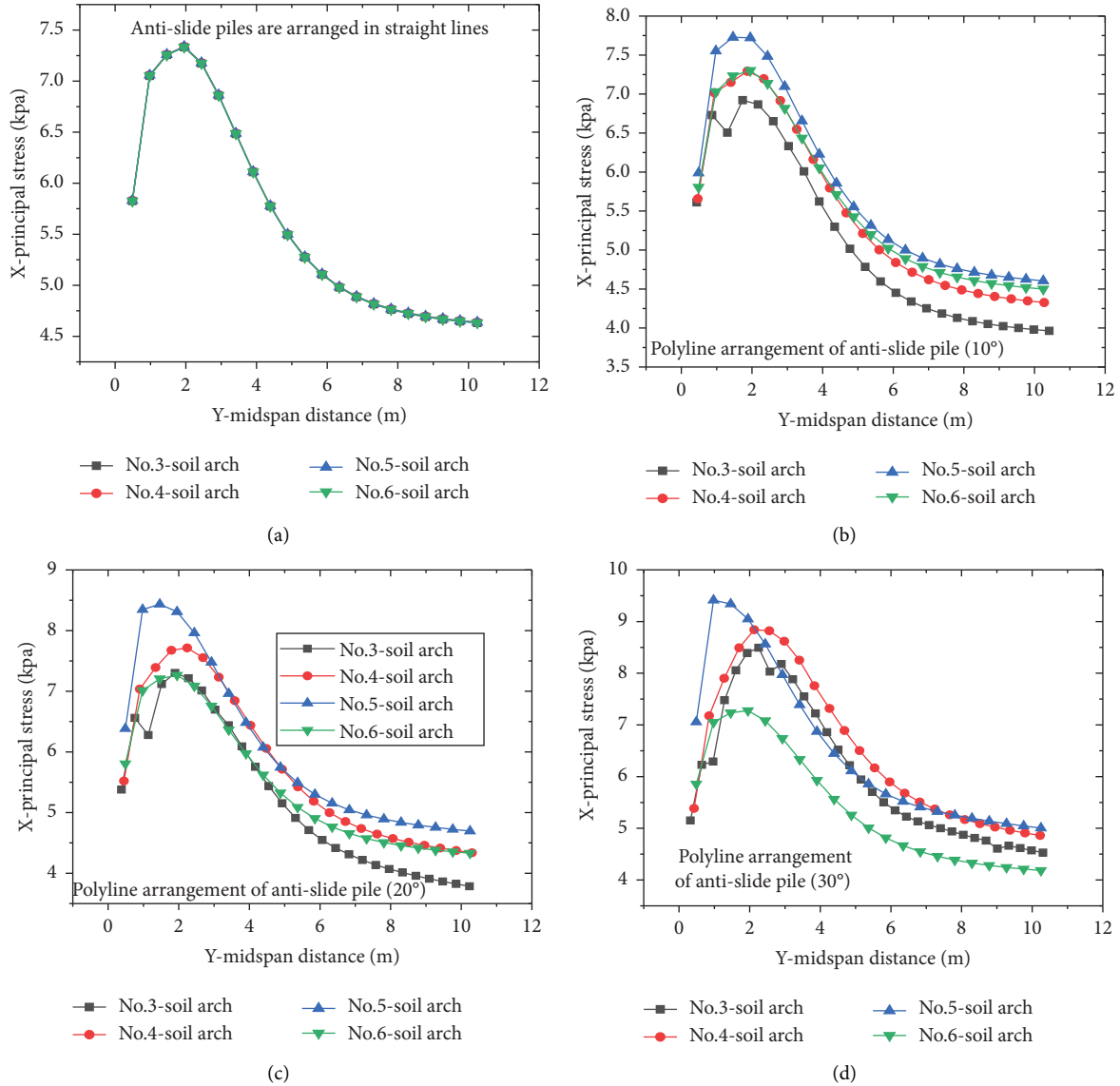


FIGURE 13: Comparisons among principal stress curves in the X direction.

in the stress curves, the inscribed slopes of the curves increase, the abrupt changes of Y-directional principal stresses are obvious, and the soil arching effect is enhanced. Regarding the Y-directional principal stress distribution of 6# soil arch, the Y-directional principal stress at the arch crown somewhat increases under polyline pile arrangement, despite a smaller increase than that of the 5# soil arch. The peak point position for 6# arch is consistent with that under a

straight line arrangement, and the soil arching effect and its range of action are fundamentally unchanged.

Table 3 lists the peak and vector height statistics for the X-directional principal stresses of soil arches, whereas Figures 13 and 14 separately depict the X-directional principal stress distributions of different soil arches under polyline pile arrangement and the X-directional principal stress variations of soil arches at different pile layout angles.

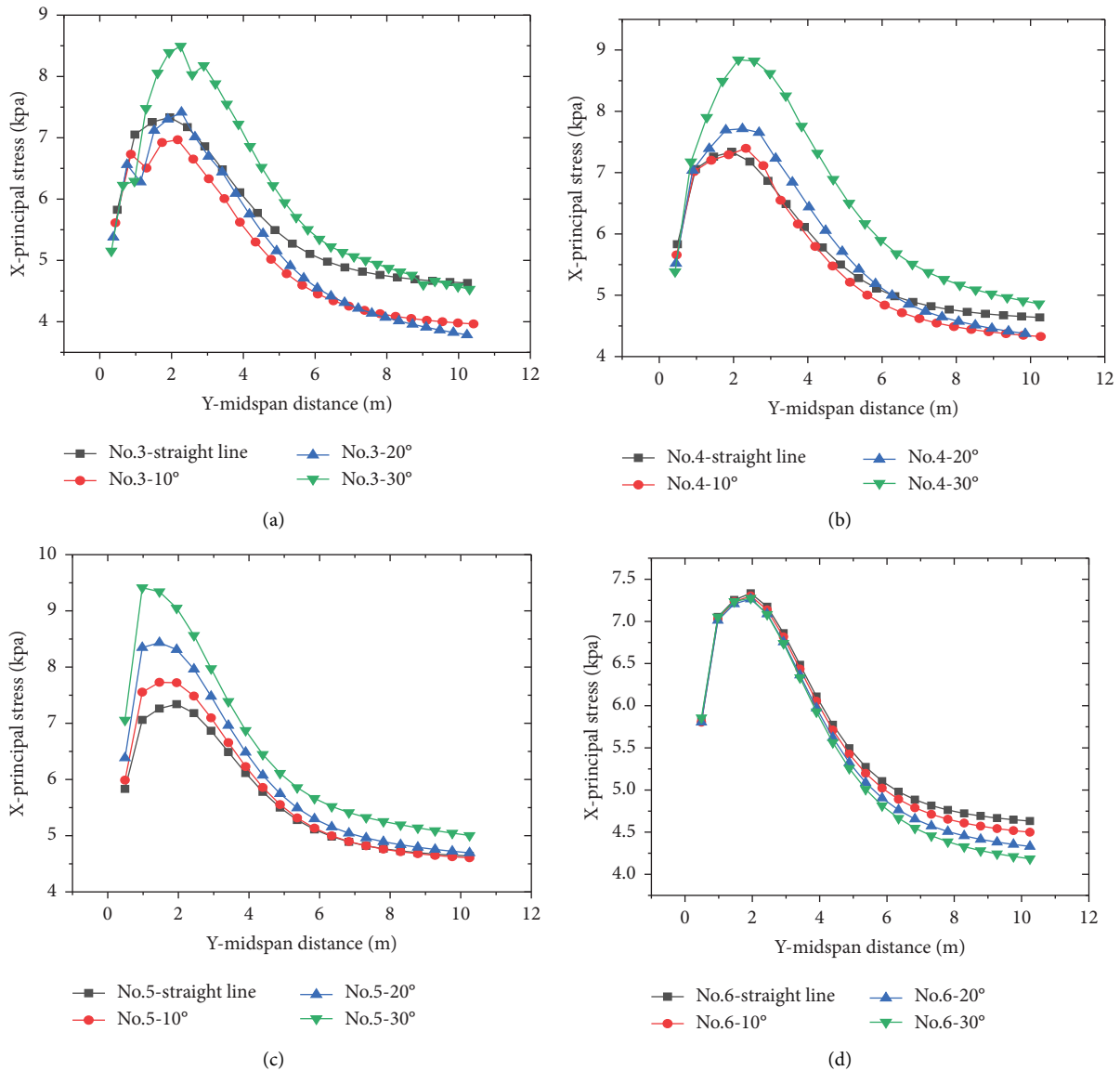


FIGURE 14: X-directional principal stress curves on the midspan symmetry planes of soil arches under polyline pile arrangements.

According to Figure 13, under polyline pile arrangement, the principal stresses in the X direction are overall large in the middle and small on two sides, and maximum principal stress in the X direction is noted at the 5# soil arch. Suggestively, the extrusion effect between soil particles becomes stronger as the distance to the inflection point becomes closer, and the stress concentration becomes obvious, which is detrimental to the structural safety of the antislide pile at the inflection point.

It is clear from Figure 14 that with the increase in pile layout angle, the X -directional principal stresses at the midspan of 3#, 4#, 5#, and 6# soil arches increase continuously, indicating that under polyline pile arrangement, the extrusion effect between soil particles is enhanced with the increasing layout angle, and the stress concentration becomes ever obvious, which is detrimental to the structural safety of antislide piles. Based on the vector height changes of soil arches, the soil arch vector heights show uneven

distribution under polyline layout when compared to the straight line layout, with those on the “section oblique to thrust” greater than those on the “section orthogonal to thrust.” That is, the 3# and 4# soil arches exhibit larger action ranges than the 5# and 6# soil arches, showing agreement with the Y -directional principal stress distributions in Figure 11.

4. Analysis of a Typical Landslide Case

The Dawanjiang landslide is located in the southwest of the Dawanjiang formation in Banxing village, Mengding town, Gengma county, with a distribution elevation range of 461–475 m. The landslide exhibits a “gentle-steep-gentle” stepped landform longitudinally. The trailing and leading edges are rather gentle, with slopes of 2–8°, while at the landslide position, the slopes are relatively steep, which vary from 15° to 45°. The landslide has a main sliding direction of



FIGURE 15: Aerial view of the Dawanjiang landslide.

176° , and an arched plane shape. Approximately, its average length is 50 m, average width is 60 m, overall area is $3,000 \text{ m}^2$, average thickness is 5 m, and overall volume $1.5 \times 10^4 \text{ m}^3$. As a small shallow-layer soil landslide, it directly threatens the safety of 9 households (45 people) and 12 buildings in Dawanjiang village Figure 15.

Borehole exposure results show that the soil exposed in the landslide site is mainly Quaternary loose deposits, which, from top to bottom, are the Quaternary artificial layer (Q_4^{ml}), the Quaternary diluvial layer (Q_4^{dl}), and the Quaternary alluvial-proluvial layer (Q_4^{al+pl}). Lithologically, the soil comprises clay and silty clay, with strong hydrophilicity. After the surface water seeps along the soil body, it easily forms a saturated water weakness belt with low shear strength within a certain depth. The underlying bedrock in the landslide site is the limestone of lower Permian Yongde formation (P_{1y}), which is not exposed on the surface.

Tensile cracks L1 with good continuity and maximum widths of 2–10 cm are formed around the trailing edge of the landslide, which is locally dislocated to form 0.1–1.0 m rear wall of the landslide Figure 16. Meanwhile, bulging cracks L2 with good continuity are formed on the leading edge of the landslide Figure 17. Field investigation finds that the landslide has a clear boundary between its east and west sides.

The Dawanjiang landslide is a soil landslide Figure 18. According to the sliding surface exposed by the boreholes, the stability coefficient of the landslide is calculated by the transfer coefficient method. The relevant parameters are: weights of slide body (1) Natural weight: 18.2 kN/m^3 ; (2) Saturated weight: 19.0 kN/m^3 . Table 4 lists the values and calculations of geotechnical parameters.

As revealed by the stability calculations, the safety factor of the landslide under natural conditions is 1.12, and the landslide is in a basically stable state. Under natural + rainstorm conditions, the landslide has a stability factor of 0.92, which is in an unstable state and requires management.

Regarding the landslide control scheme, support with antisliding piles is adopted. The antisliding piles were arranged in a straight line and in a polyline for comparative analysis.



FIGURE 16: Trailing edge boundary of the landslide.



FIGURE 17: Leading edge bulging of the landslide.

Under a straight line layout, the piles are arranged at the leading edge of the landslide, while under a polyline layout, the piles are arranged according to the terrain lines. Since the sliding surface of the landslide is 5–6 m in depth, the length of antisliding piles is set at 9 m. The length of the anchoring section is 1/3 of the pile length, and the pile spacing is set at 5 m. Figure 19 displays the plan layout of the antisliding piles. Based on the actual terrain changes, the backfill back pressure is involved in both the straight line and polyline pile layouts, albeit with differences in their quantity.

During calculation, the parameters of antisliding piles are described as follows: the cross-sectional area = 3 m^2 , the elastic modulus $E = 20 \text{ GPa}$, the Poisson's ratio = 0.2, the X-axis polar moment of inertia = 7, the Y-axis polar moment of inertia = 5, the Z-axis polar moment of inertia = 3, the stiffness on unit length of shear coupling spring $K_s = 1 \times 10^8 \text{ kN/m}$, the cohesive force on unit length of shear coupling spring = $2 \times 10^4 \text{ kPa}$, the internal friction angle on

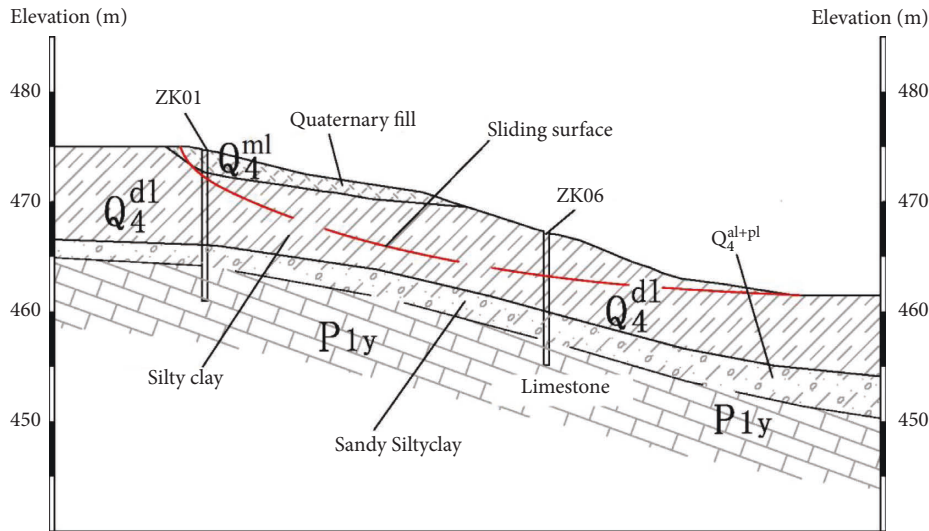


FIGURE 18: Engineering geological profile of the landslide.

TABLE 4: Physicomechanical parameters of landslide and stability calculations.

| Calculation condition | Shear strength index | | | | (kN/m) overall sliding force | (kN/m) overall sliding resistance | Stability factor |
|-----------------------|----------------------|---------------|-----------|---------------|------------------------------|-----------------------------------|------------------|
| | Natural | | Saturated | | | | |
| | C (kPa) | φ (°) | C (kPa) | φ (°) | | | |
| Natural | 9 | 2.5 | | | 478.6 | 535.33 | 1.12 |
| Natural + rainstorm | | | 8 | 2.5 | 501.41 | 461.23 | 0.92 |

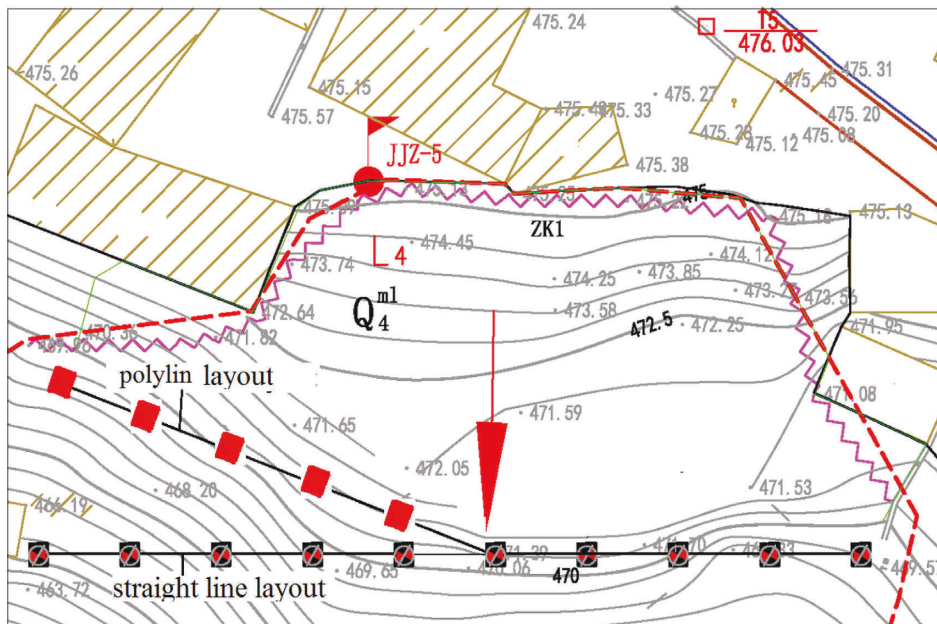


FIGURE 19: Plane layout of antislide piles arranged in a straight line and in a polyline.

unit length of shear coupling spring = 15° , the stiffness on unit length of normal coupling spring $K_s = 1 \times 10^8$ kN/m, the cohesive force on unit length of normal coupling spring = 2×10^4 kPa, and the internal friction angle on unit length of normal coupling spring = 15° .

4.1. Analysis of Landslide Displacement. Figures 20 and 21 separately present the landslide displacement nephogram under the straight line and polyline pile arrangements. In terms of displacement field distribution, the straight line layout can effectively prevent the downward sliding of

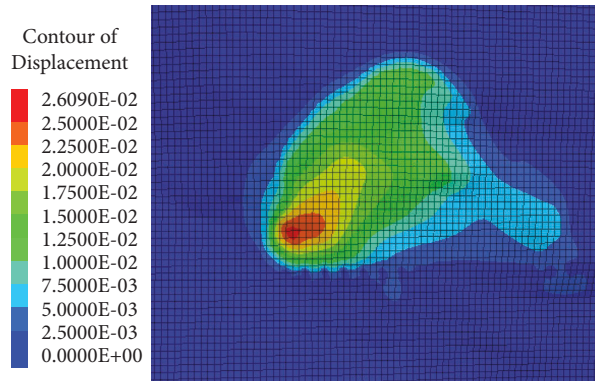


FIGURE 20: Displacement nephogram under polyline pile reinforcement.

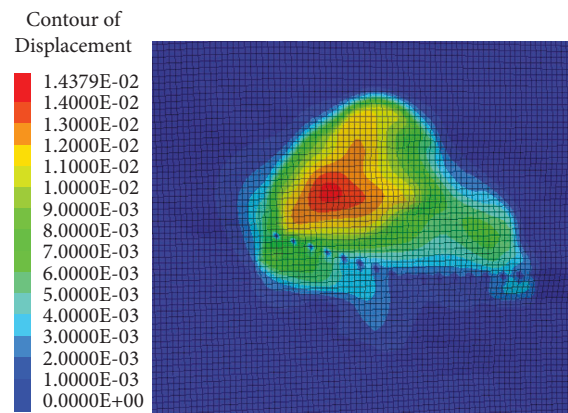


FIGURE 21: Displacement nephogram under straight line pile reinforcement.

landslide since the antislides piles are arranged at the leading edge, where the displacement of soil in front of piles is basically 0. Contrastively, in the case of polyline pile layout, although the antislides piles can prevent the downward sliding of soil behind piles since they are arranged along the terrain lines, the soil in front of piles in the polyline layout zone is still at the downward sliding risk.

4.2. Analysis of Landslide Plastic Zone. During the calculation with Mohr–Coulomb plasticity model in FLAC3D, if the stress in the unit body reaches the Mohr–Coulomb yield criterion, this area will be damaged or be a potential damage area, which is defined as the plastic zone. Depending on the failure mechanism, the plastic zone can be divided into the shear failure zone and the tensile failure zone. During the calculation, some areas may have entered the failure state, and then retreated due to the stress redistribution, which is marked as shear-p or tension-p on the plastic zone diagram. Meanwhile, on the diagram of area currently in a failure state, this is marked as shear-n or tension-n, so the analysis of the plastic zone is based primarily on the distribution area of shear-n and tension-n. The larger the plastic zone area, the larger the failure area of landslide, and vice versa. For the convenience of analysis, the color of the areas, which had entered the failure state but later retreated with the progress

of calculation, is adjusted to the same color as the background meshes.

Figures 22 and 23 separately depict the plastic zone distributions of the landslide under the straight line and polyline pile layouts. Comparison between the two figures reveals that in the case of polyline layout, both the tensile and shear failure zones of the landslide are larger than those under the straight line layout. For the site of soil before piles, in particular, the shear failure area of soil body is significantly larger than that under a straight line layout.

4.3. Comparative Analysis of Internal Force Distribution of Piles. Figures 24 and 25 separately display the bending moment and shear force distribution nephodiagram of antislides piles under straight line pile arrangement. Clearly, in the case of straight line layout, the antislides piles have a maximum bending moment of 1484.8 kN m and a maximum shear force of about 330 kN. The bending moment and shear force distributions at various pile positions are relatively uniform.

Figures 26 and 27 separately present the bending moment and shear force distribution nephogram of antislides piles under polyline pile arrangement. Clearly, both the pile bending moments and shear forces increase, whose distributions are nonuniform. The maximum bending moment is

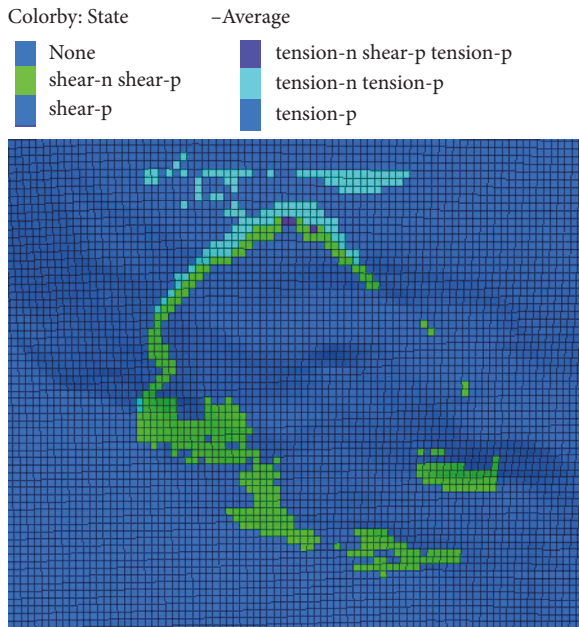


FIGURE 22: Plastic zone distribution under straight line layout.

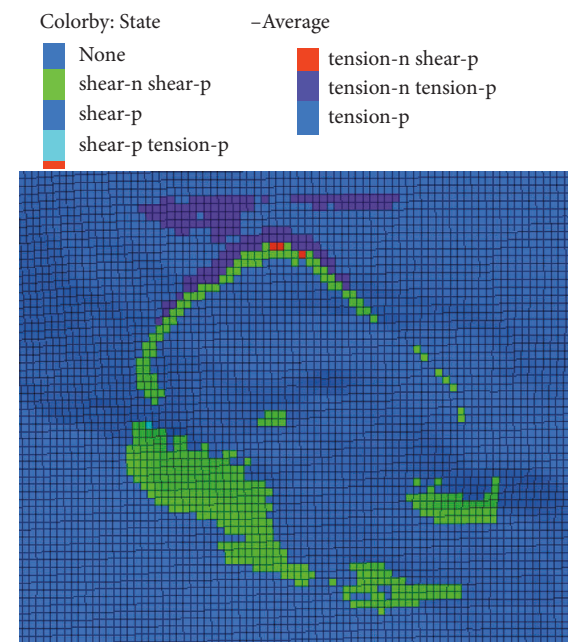


FIGURE 23: Plastic zone distribution under polyline layout.

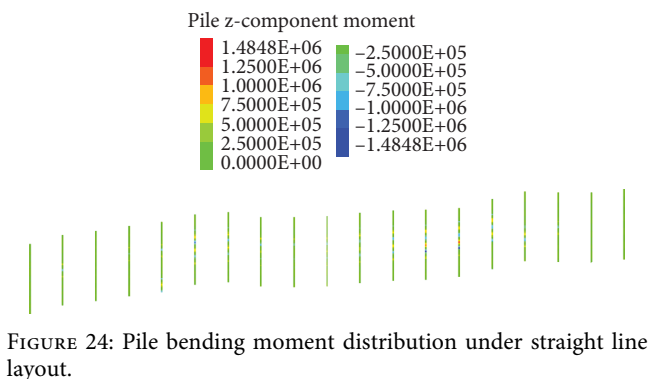


FIGURE 24: Pile bending moment distribution under straight line layout.

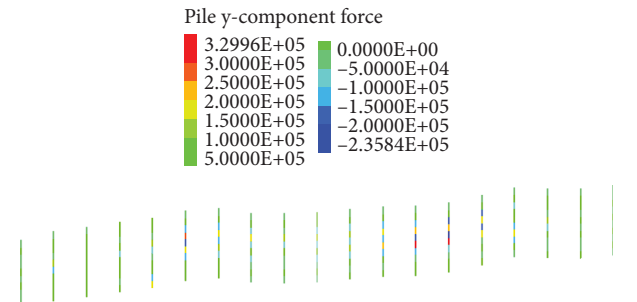


FIGURE 25: Pile shear force distribution under straight line layout.

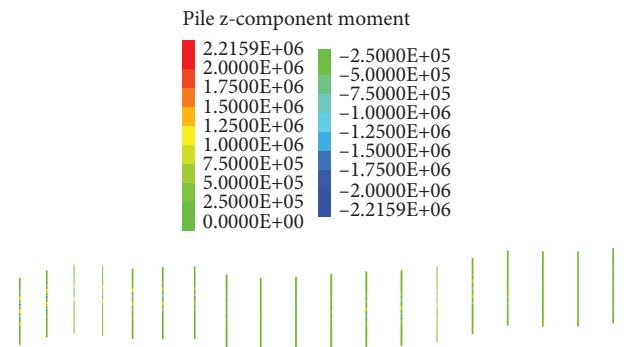


FIGURE 26: Pile bending moment distribution under polyline layout.

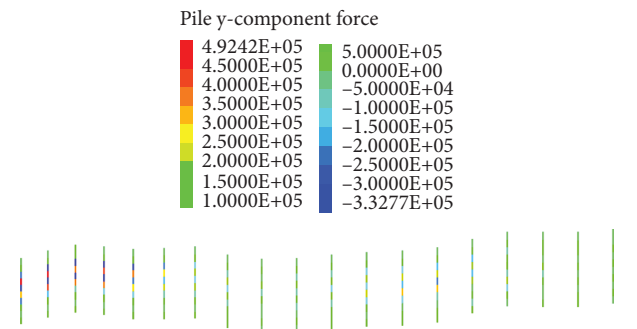


FIGURE 27: Pile shear force distribution under polyline layout.

2,215.9.4 kN m, whereas the maximum shear force is 492.4 kN, showing markedly larger values than those under a straight line layout. Based on these, it can be confirmed that when the antislid piles of identical size are used to reinforce the same landslide, the polyline layout poses a greater risk to the pile's structural safety.

5. Conclusions

Through numerical simulation, this study comparatively analysis the soil arching effect characteristics of cantilever antislid piles arranged in straight lines versus polylines. In the typical case of the Dawanjiang landslide, the differences between a polyline and straight line pile layouts are verified, as well as their impacts on landslide control and the pile structure. The main conclusions are drawn as follows:

- (1) Under straight line arrangement of piles, the soil arching effect gradually weakens along the direction away from the antislide piles, and the forces and action range of soil arches at various pile positions are basically identical. This indicates that under a straight line layout, the landslide thrust is uniformly distributed at various positions, and the antislide sheet-pile walls evenly share the load, which is beneficial to the structural safety of the walls.
- (2) In the case of polyline pile arrangement, the soil pressures at the apex of soil arches within the “section oblique to thrust” decrease, while those within the “section orthogonal to thrust” increase. Such an increase is most evident for the soil arch at the inflection point. Moreover, with the increasing angle of polyline pile layout, the principal stress at the “inflection point” increases ever more evident, which is detrimental to the structural safety of the antislide sheet-pile wall at the inflection point.
- (3) The polyline pile layout has a weakening effect on the soil arching evolution in the “section orthogonal to thrust,” which though attenuates with the increasing distance. This is manifested mainly in the reduced range of soil arching effect at the “inflection point,” and the significantly increased principal stress at the arch apex. After being far away from the “inflection point,” the range of soil arching effect in the “section orthogonal to thrust” increases gradually, while the principal stress shows relative decreases until it recovers to the same value as that under the straight line layout.
- (4) The structural forces of antislide piles arranged in straight lines differ markedly from those arranged in polylines. Under a straight line layout, the bending moment and shear force distributions at various pile positions are relatively uniform. Contrastively, under polyline layout, both the bending moments and shear forces of the antislide piles increase, whose distributions are nonuniform. Suggestively, when piles of identical size are used to reinforce the same landslide, the polyline pile layout poses a greater risk to the pile’s structural safety.

Data Availability

The data used to support the findings of this study are included within the article.

Conflicts of Interest

The authors declare no conflicts of interest, financial, or otherwise.

Authors’ Contributions

A. Fayou and Xue-gang Dai contributed equally to this work.

Acknowledgments

The National Natural Science Foundation of China (Grant 42267020), the Project of High-quality Course Construction for Graduate Students of Yunnan Province in 2020 (Numerical simulation of geological engineering), and the Key Research and Development Program of Yunnan Province in 2022 (202203AC100003).

References

- [1] V. M. Ulitskii, “History of pile foundation engineering,” *Soil Mechanics and Foundation Engineering*, vol. 32, no. 3, pp. 110–114, 1995.
- [2] V. M. Ponin, V. A. Il’yashenko, B. V. Goncharov, and G. S. Kolesnik, “Prospects for the development of pile foundation engineering in the ministry of industrial construction of the USSR,” *Soil Mechanics and Foundation Engineering*, vol. 19, no. 6, pp. 244–247, 1982.
- [3] S. P. 24.13330, “Pile Foundations. Updated version of SNiP 2.02.03-85 [in Russian],” Moscow, 2011.
- [4] V. I. Golik, C. B. Kongar Syuryun, A. Michalek, P. Pires, and A. Rybak, “Ground transmitted vibrations in course of innovative vinyl sheet piles driving,” *Journal of Physics: Conference Series*, vol. 1921, no. 1, Article ID 012083, 2021.
- [5] A. Herbut, M. M. Khairutdinov, C. Kongar-Syuryun, and J. Rybak, “The surface wave attenuation as the effect of vibratory compaction of building embankments,” *IOP Conference Series: Earth and Environmental Science*, vol. 362, no. 1, Article ID 012131, 2019.
- [6] P. Dobrzycki, A. L. Ivannikov, J. Rybak, V. O. Shkodkina, and Y. S. Tyulyaeva, “The impact of Rapid Impulse Compaction (RIC) of large non-cohesive material deposits on the surrounding area,” *IOP Conference Series: Earth and Environmental Science*, vol. 362, no. 1, Article ID 012132, 2019.
- [7] F. Nadim, C. Jaedicke, H. Smebye, and B. Kalsnes, “Assessment of global landslide hazard hotspots,” in *Landslides: Global Risk Preparedness*, K. Sassa, B. Rouhban, S. Briceño, M. McSaveney, and B. He, Eds., pp. 59–71, Springer, Berlin, Heidelberg, 2013.
- [8] E. Sanz-Pérez, I. Menéndez-Pidal, A. Lomoschitz, and R. Galindo-Aires, “The pico de navas slump (Burgos, Spain): a large rocky landslide caused by underlying clayey sand,” *Journal of Iberian Geology*, vol. 42, no. 1, pp. 55–68, 2016.
- [9] K. S. Shadunts and S. I. Matsii, “Interaction between pile rows and sliding soil,” *Soil Mechanics and Foundation Engineering*, vol. 34, no. 2, pp. 35–40, 1997.
- [10] B. Yuan, M. Chen, W. Chen, Q. Luo, and H. Li, “Effect of pile-soil relative stiffness on deformation characteristics of the laterally loaded pile,” *Advances in Materials Science and Engineering*, vol. 2022, pp. 1–13, 2022.
- [11] A. Fa-you, “Investigating the effect of the rock-socketed depth of the hinged cable-anchored pile on the earthquake response characteristics of supporting structures,” *Advances in Civil Engineering*, vol. 2022, 2022.
- [12] Y. Wang and M. Han, “Optimal design of slope reinforcement by a new developed polymer micro anti-slide pile in case of emergency and disaster relief,” *Natural Hazards*, vol. 112, no. 1, pp. 899–917, 2022.
- [13] R. Shams and A. Hussain, “Analysis of effect of anti-slide pile on stability of slopes,” in *Advances in Geotechnics and Structural Engineering. Lecture Notes in Civil Engineering*, S. Kumar Shukla, S. N. Raman, B. Bhattacharjee, and

- J. Bhattacharjee, Eds., vol. 143, pp. 237–246, Springer, Singapore, 2021.
- [14] C. Li, J. Wu, H. Tang, J. Wang, F. Chen, and D. Liang, “A novel optimal plane arrangement of stabilizing piles based on soil arching effect and stability limit for 3D colluvial landslides,” *Engineering Geology*, vol. 195, no. 06, pp. 236–247, 2015.
- [15] C. Li, W. Chen, Y. Song, W. Gong, and Q. Zhao, “Optimal location of piles in stabilizing slopes based on a simplified double-row piles model,” *KSCE Journal of Civil Engineering*, vol. 24, no. 2, pp. 377–389, 2020.
- [16] Wq. Liu, Q. Li, J. Lu, Cd. Li, Wm. Yao, and Jb. Zeng, “Improved plane layout of stabilizing piles based on the piecewise function expression of the irregular driving force,” *Journal of Mountain Science*, vol. 15, no. 4, pp. 871–881, 2018.
- [17] H. Zhang, C. Li, W. Yao, and J. Long, “A novel approach for determining pile spacing considering interactions among multilayered sliding masses in colluvial landslides,” *KSCE Journal of Civil Engineering*, vol. 23, no. 9, pp. 3935–3950, 2019.
- [18] H. Zhang, J. Chen, and M. Xu, “The determination of rational spacing of anti-slide piles and soil pressure on pile sheet based on soil arching effect,” *Geotechnical & Geological Engineering*, vol. 40, no. 5, pp. 2857–2866, 2022.
- [19] S. J. Li, J. Chen, and C. Lian, “Mechanical model of soil arch for interaction of piles and slope and problem of pile spacing,” *Rock and Soil Mechanics*, vol. 31, no. 5, pp. 1352–1358, 2010, (in Chinese).
- [20] J. I. A. Ha-ili, C. Wang, and L. I. Jiang-hong, “Discussion on some issues in theory of soil arch,” *Journal of Southwest Jiaotong University*, vol. 38, no. 4, pp. 398–402, 2003, (in Chinese).
- [21] I. Roberts, “Determination of the vertical and lateral pressures of granular substances,” *Proceedings of the Royal Society of London*, vol. 36, no. 228-231, pp. 225–240, 1884.
- [22] K. Terzaghi, *Theoretical Soil Mechanics*, John Wiley & Sons, 1943.
- [23] W. L. Wang and B. C. Yen, “Soil arching in slopes,” *Journal of the Geotechnical Engineering Division*, vol. 100, no. 1, pp. 61–78, 1974.
- [24] S. Zhang, C. Li, H. Qi, X. Chen, and S. Ma, “Soil arch evolution characteristics and parametric analysis of slope anchored anti-slide pile,” *KSCE Journal of Civil Engineering*, vol. 25, no. 11, pp. 4121–4132, 2021.
- [25] C. Li, H. Tang, X. Hu, and L. Wang, “Numerical modelling study of the load sharing law of anti-sliding piles based on the soil arching effect for erliban landslide, China,” *KSCE Journal of Civil Engineering*, vol. 17, no. 6, pp. 1251–1262, 2013.
- [26] Z. Liu, Z. Yan, X. Wang, J. Li, and Z. Qiu, “Effect of the inclined pile-soil arch in a soil landslide reinforced with anti-sliding piles,” *Natural Hazards*, vol. 106, no. 3, pp. 2227–2249, 2021.
- [27] P. J. Bosscher and D. H. Gray, “Soil arching in Sandy slopes,” *Journal of Geotechnical Engineering*, vol. 112, no. 6, pp. 626–645, 1986.
- [28] D. Mujah, H. Hazarika, N. Watanabe, and F. Ahmad, “Soil arching effect in sand reinforced with micropiles under lateral load,” *Soil Mechanics and Foundation Engineering*, vol. 53, no. 3, pp. 152–157, 2016.
- [29] K. Deb, “A mathematical model to study the soil arching effect in stone column-supported embankment resting on soft foundation soil,” *Applied Mathematical Modelling*, vol. 34, no. 12, pp. 3871–3883, 2010.
- [30] X. Zhao, K. Li, and D. Xiao, “A simplified method to analyze the load on composite retaining structures based on a novel soil arch model,” *Bulletin of Engineering Geology and the Environment*, vol. 79, no. 7, pp. 3483–3496, 2020.
- [31] C. Yun-min, C. Wei-ping, and C. Ren-peng, “An experimental investigation of soil arching within basal reinforced and unreinforced piled embankments,” *Geotextiles and Geomembranes*, vol. 26, no. 2, pp. 164–174, 2008.
- [32] R. Rui, J. Han, S. J. M. van Eekelen, and Y. Wan, “Experimental investigation of soil-arching development in unreinforced and geosynthetic-reinforced pile-supported embankments,” *Journal of Geotechnical and Geoenvironmental Engineering*, vol. 145, no. 1, Article ID 04018103, 2019.
- [33] C. Xu, L. Liang, Q. Chen, W. Luo, and Y. F. Chen, “Experimental study of soil arching effect under seepage condition,” *Acta Geotechnica*, vol. 14, no. 6, pp. 2031–2044, 2019.
- [34] T. Yang, Z. Lu, J. Ni, and G. Wang, “3D finite-element modelling of soil arch shape in a piled embankment,” *Proceedings of the Institution of Civil Engineers - Geotechnical Engineering*, vol. 172, no. 3, pp. 255–262, 2019.
- [35] N. Bao, J. Wei, J. f Chen, and P. Wei, “2D and 3D discrete numerical modelling of soil arching,” *Journal of Zhejiang University - Science*, vol. 21, no. 5, pp. 350–365, 2020.
- [36] H. J. Lai, J. J. Zheng, M. J. Cui, and J. Chu, “Soil arching” for piled embankments: insights from stress redistribution behaviour of DEM modelling,” *Acta Geotechnica*, vol. 15, no. 8, pp. 2117–2136, 2020.
- [37] H. L. Jia, C. H. Wang, and L. I. Jiang-Hong, “Discussion on some issues in theory of soil arch,” *Journal of Southwest Jiaotong University*, vol. 38, no. 4, pp. 398–402, 2003, (in Chinese).
- [38] X. Lu, S. Mengen, and P. Wang, “Numerical simulation of the composite foundation of cement soil mixing piles using FLAC3D,” *Cluster Computing*, vol. 22, no. S4, pp. 7965–7974, 2018.
- [39] J. J. Wu, Y. Li, Q. G. Cheng, H. Wen, and X. Liang, “A simplified method for the determination of vertically loaded pile-soil interface parameters in layered soil based on FLAC3D,” *Frontiers of Structural and Civil Engineering*, vol. 10, no. 1, pp. 103–111, 2015.